Vorinostat Rescues SQSTM1 Palmitoylation and Restores Dysfunctional Autophagy in Huntington Disease

Yasmeen Alshehabi, Fatima Abrar, Milena Rabu, Anthony Dang, Firyal Ramzan, and Dale D. O. Martin

NeurdyPhagy Lab, Department of Biology, Faculty of Science, University of Waterloo, Waterloo, ON, Canada

Running title: Vorinostat restores autophagy in HD

Correspondance: Dale D. O. Martin, dale.martin@uwaterloo.ca

Keywords: neurodegeneration, autophagy, SQSTM1, p62, Vorinostat, Huntington Disease, S-acylation, palmitoylation

Abstract

Protein mislocalization, impaired autophagy, and protein aggregation are central features of Huntington disease (HD), yet therapeutic strategies that simply stimulate autophagy risk exacerbating dysfunction in an already compromised pathway. We previously demonstrated that palmitoylation of the autophagy receptor SQSTM1/p62 is reduced in HD patient brains and YAC128 mice, contributing to defective cargo loading and accumulation of mutant huntingtin (mHTT) aggregates. Here, we identify the FDA-approved histone deacetylase inhibitor Vorinostat (also known as suberoylanilide hydroxamic acid; SAHA) as a small molecule that restores SQSTM1 palmitoylation and autophagic function in HD models. Using acyl-biotin exchange and click chemistry assays, we show that Vorinostat selectively increases SQSTM1 palmitoylation without altering total protein palmitoylation. In turn, Vorinostat enhances autophagic flux, decreases SQSTM1 levels, increases LC3-II, and promotes colocalization of SQSTM1, mHTT, and lysosomes, indicating improved cargo delivery and degradation. Importantly, systemic administration of Vorinostat crosses the blood-brain barrier and restores SQSTM1 palmitoylation in YAC128 mouse cortices. Mechanistically, Vorinostat may function through dual pathways: partial inhibition of depalmitoylating enzymes and transcriptional regulation of palmitoylation machinery. These findings build on our identification of SQSTM1 palmitoylation as a therapeutic target for HD and repositions Vorinostat as a candidate modifier of autophagy dysfunction and palmitoylation impairment in HD.

32 # 1. Introduction

33 Protein aggregation is a hallmark of several neurodegenerative diseases, including Huntington disease
34 (HD), amyotrophic lateral sclerosis (ALS), Alzheimer disease (AD), and Parkinson disease (PD)[1–3]. The
35 intracellular pathway responsible for clearing aggregates, known as autophagy, is often impaired in
36 these devastating conditions[1]. As a result, autophagy is an attractive therapeutic target for clearing the
37 toxic aggregates that exacerbate disease progression. However, only stimulating autophagy is
38 insufficient, as it places additional stress on a system that is already compromised. Therefore,
39 addressing the underlying defects, in conjunction with increasing autophagy, is essential for effective
40 therapeutic intervention.

41

42 Macroautophagy, henceforth referred to as autophagy, involves the loading of cargo, such as toxic or
43 aggregated proteins and damaged organelles, into a double-membrane structure known as a
44 phagophore, which seals to form an autophagosome[4] (Figure 1B). This autophagosome is then
45 transported and fused with a lysosome to form the ultimate structure known as an autophagolysosome
46 where the cargo is degraded with hydrolases[4]. The cargo-loading step is crucial, wherein sequestosome
47 1 (SQSTM1; commonly known as p62) binds ubiquitinated cargo destined for degradation and delivers it
48 to lipidated microtubule-associated protein 1 light chain 3 (LC3-II), located on both sides of the
49 phagophore membrane[4]. In HD, autophagy is dysfunctional at several steps (Figure 1C)[5]. Critically, there
50 is a cargo-loading failure that leads to an accumulation of empty autophagosomes and protein
51 aggregates[6,7].

52

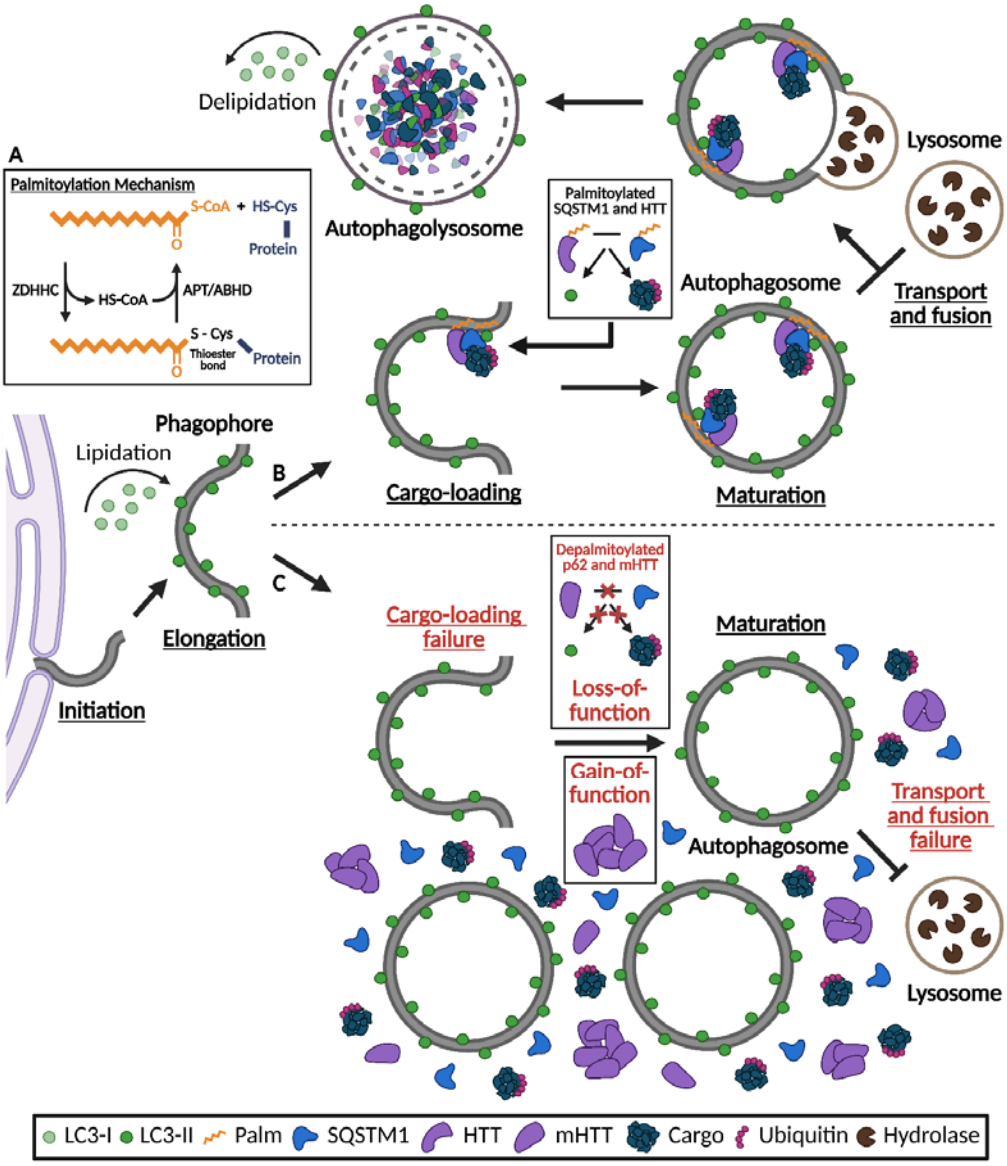

Figure 1 – SQSTM1 and HTT palmitoylation may support healthy autophagy, and its deficiency may contribute to autophagic dysfunction in HD. (A) Palmitoylation involves the formation of a thioester bond between palmitoyl-CoA and a free cysteine residue in a protein via palmitoyl acyltransferases (ZDHHCs). Depalmitoylation involves the cleavage of a thioester bond via acyl protein thioesterases (APTs) or α/β-hydrolase domain enzymes (ABHDs). **(B)** LC3-I undergoes lipidation to form LC3-II, located on both sides of the phagophore membrane. LC3-II then recruits SQSTM1, which is bound to the ubiquitinated cargo destined for degradation. HTT acts as a scaffold to support the function of SQSTM1. We predict that the palmitoylation of SQSTM1 and HTT plays an important role in their delivery of cargo to the phagophore membrane. Next, the phagophore expands around the cargo and closes to form a sealed autophagosome, which then fuses with a lysosome to form an autophagolysosome. All the contents inside this vesicle are degraded by hydrolytic enzymes, and LC3-II bound to the outside of the double-membrane is released back to the cytosol. **(C)** In HD, there is a defect at the cargo-loading step leading to an accumulation of mHTT aggregates and empty autophagosomes. We predict that this cargo-loading failure is at least partially the result of a reduction in SQSTM1 and HTT palmitoylation. Figure created with Biorender.

69 HD is a neurodegenerative disease with devastating affects on cognition and motor function[8]. HD is an
70 autosomal dominant, monogenic disease caused by a mutation in exon 1 of the huntingtin gene (*HTT*)
71 that encodes a cytosine-adenine-guanine (CAG) repeat expansion (*i.e.,* 36 to 39 CAG repeats for partial
72 HD penetrance; 40 or more repeats for full HD penetrance) resulting in a polyglutamine expansion in the
73 huntingtin protein (HTT)[9,10]. In healthy conditions, HTT is ubiquitous and involved in many cellular
74 processes[11], including autophagy, in which HTT functions as a scaffold, binding to SQSTM1 and
75 ubiquitinated cargo to support the function of SQSTM1 in cargo-loading[12–14]. However, cargo-loading is
76 impaired in HD[6,7], which may be at least partly due to reduced palmitoylation of SQSTM1 and mHTT. We
77 have shown that SQSTM1 palmitoylation plays an important role in cargo-loading and is required for
78 SQSTM1 localization to autophagosomes[15,16]. Notably, SQSTM1 palmitoylation is significantly reduced in
79 the brains of HD patients and YAC128 mice[15,16]. In turn, increasing SQSTM1 palmitoylation using broad
80 palmitoylation inhibitor Palmostatin B improved HTT and SQSTM1 localization to autophagosomes[15,16].
81 Moreover, the Hayden group has shown that mHTT palmitoylation is reduced in HD mouse models and
82 further decreases with increasing age and CAG repeat length[17,18]. Subsequently, Palmostatin B restored
83 mHTT palmitoylation and thus mHTT aggregation and cytotoxicity in HD mouse model primary
84 neurons[18].
85
86 Palmitoylation, the most common form of S-acylation, is the reversible post-translational addition of a
87 16-carbon fatty acid to a cysteine residue via a thioester bond[19] (Figure 1A). Due to its reversibility and
88 hydrophobicity, palmitoylation allows selective and dynamic targeting of soluble proteins to membranes
89 and thus plays a key role in regulating protein trafficking[19]. Palmitoylation is mediated by 23 palmitoyl
90 acyltransferases (ZDHHCs) in humans, whereas the reverse reaction is mediated by acyl protein
91 thioesterase (APT), palmitoylprotein thioesterase (PPT), and α/β-hydrolase domain (ABHD) enzymes[20].
92

93 The Hayden group has shown that HTT is palmitoylated by ZDHHC13 and ZDHHC17, and depalmitoylated
94 by APT1 and APT2[17,18,21,22]. Importantly, HD is linked to decreased ZDHHC17 activity and increased APT1
95 activity[23]. Furthermore, the Yang group has shown that SQSTM1 is depalmitoylated by APT1[15,24]. In turn,
96 the Saudou group demonstrated that APT1 activity is increased in HD and specific inhibition of APT1
97 using ML348 is protective in an HD mouse model[25]. Consequently, APT1 may be a therapeutic target in
98 HD. Therefore, the identification of a small molecule which can increase SQSTM1 palmitoylation holds
99 therapeutic promise for HD, rescuing cargo-loading in autophagy, and in turn, reducing mHTT
100 aggregation and toxicity. Through a high-throughput screening of FDA-approved drugs, we identified
101 Vorinostat, also known as suberoylanilide hydroxamic acid (SAHA), as a potential candidate for
102 increasing SQSTM1 palmitoylation[26]. Vorinostat is primarily known as a blood-brain barrier (BBB)
103 permeable inhibitor of lysine deacetylases (KDACs), more commonly known as histone deacetylases
104 (HDACs), which catalyze the removal of acetyl groups (*i.e.,* deacetylation) from lysine residues on
105 histone and/or non-histone proteins[27,28]. Herein, we report that Vorinostat significantly increases
106 SQSTM1 palmitoylation, increases and enhances autophagic flux, and may function as a
107 depalmitoylating enzyme inhibitor and a transcriptional regulator. Importantly, we found that
108 Vorinostat crosses the blood-brain barrier and restores SQSTM1 palmitoylation in YAC128 HD mouse
109 model brains.
110

111 ## 2. Materials and Methods

112 ### 2.1 Cell Culture

113 HeLa cells were grown at 37°C in 5% CO_2 in Dulbecco's Modified Eagle Medium (DMEM; Wisent #319-
114 015 CL) supplemented with 10% fetal bovine serum (FBS), 2 mM L-glutamine, 1 mM sodium pyruvate,
115 1X penicillin-streptomycin. Cells were seeded at 170,000 cells per 6 cm plate for biochemistry
116 experiments and 75,000 cells per well onto 0.01 mg/mL poly-D-lysine coated coverslips (#1.5; VWR) in 6-
117 well plates for microscopy experiments. The next day, cells were transfected with 10 µg of plasmid DNA
118 using calcium phosphate precipitation and incubated for 2 hours. The transfection mix contained 1X
119 HEPES-buffered saline (HBS) and 122 mM $CaCl_2$. The media was replaced 2 hours post transfection.
120 Where indicated, drugs were added to transfected cells immediately following the media change and
121 cells were processed 18 hours post transfection (*i.e.,* 16-hour drug incubation). For non-transfected
122 cells, indicated drugs were added for 16 hours prior to processing. Drugs were added at the listed
123 concentrations: 10 µM Vorinostat (Sigma #SML0061), 10 µM ML348 (Cayman #18523), 10 µM
124 Palmostatin B (PalmB; Millipore #178501), 50 µM 2-bromopalmitate (2BP; Sigma #238422), and/or 100
125 nM Bafilomycin A1 (BafA1; Millipore #196000). All drugs were dissolved in dimethyl sulfoxide (DMSO),
126 except for 2BP which was dissolved in ethanol.

127 ### 2.2 Click Chemistry Assay

128 Cell labeling and click chemistry were performed as previously described[29]. Briefly, the alkynyl palmitate
129 fatty acid analog (Click Chemistry Tools #CCT-1165) was saponified in potassium hydroxide and
130 conjugated to fatty-acid free bovine serum albumin (BSA). Cells were then deprived of lipids in DMEM
131 supplemented with 5% charcoal-stripped FBS (Wisent #080-710), 2 mM L-glutamine, 1 mM sodium
132 pyruvate, 1X penicillin-streptomycin, and incubated with the alkynyl palmitate for 4 hours, after which
133 cells were lysed in modified RIPA buffer (50 mM HEPES pH 7.4, 150 mM NaCl, 2 mM $MgCl_2$, 1% Igepal
134 CA-630, 0.5% sodium deoxycholate, 0.1% SDS). Iodoacetamide was added to each sample to block free

135 cysteine residues. Finally, lysates were subjected to click chemistry with biotin-azide (Click Chemistry
136 Tools #CCT-1488), tris-hydroxypropyl triazolyl methylamine (THPTA; Click Chemistry Tools #CCT-1010),
137 copper sulfate, and sodium ascorbate for 1 hour. The reaction was then ended by acetone precipitation.
138 Since we are looking at total palmitoylated protein, the affinity purification step was skipped, and the
139 protein was denatured at 95°C for 5 minutes in 1X sample loading buffer (SLB) with 20 mM dithiothreitol
140 and stored at -20°C.

141 **2.3 Acyl Biotin Exchange (ABE) Assay**

142 The acyl biotin exchange (ABE) was performed as previously described[30]. Briefly, ground cortical brain
143 tissue (approximately 30 mg) was sonicated (3x6 seconds at 20%) in ABE homogenization buffer (10 mM
144 10X phosphate buffer pH 7.4, 0.32 M sucrose, 1 mM EDTA, 6 M urea, 2.5% SDS) with 1X PIC and 20 mM
145 methyl methanthiosulfate (MMTS). Alternatively, cells were sonicated (2x6 seconds at 20%) in lysis
146 buffer (50 mM HEPES pH 7.4, 1 mM EDTA, 2% SDS) with 1X PIC and 20 mM MMTS. Lysates were
147 incubated for 30 minutes at 50°C to block free cysteine residues with MMTS. Excess MMTS was removed
148 by acetone precipitation and resuspended in 4SB (50 mM Tris pH 7.5, 5 mM EDTA, 4% SDS). Samples
149 were then incubated with 0.7 M hydroxylamine and 1 mM HPDP-Biotin (APExBIO #A8008) for 1 hour
150 rotating at room temperature to cleave thioester bonds and label newly freed cysteine residues with
151 biotin. The reaction was ended by acetone precipitation and resuspended in lysis buffer without MMTS.
152 Following protein quantification, 0.5-1 mg of protein was incubated in 150 mM NaCl dilution buffer (50
153 mM HEPES pH 7.0, 1% TX-100, 1 mM EDTA, 1 mM EGTA) with High-Capacity NeutrAvidin Agarose beads
154 (Thermo #29202) for 3 hours rotating at 4°C to bind biotinylated proteins. Following two washes with
155 0.5 M NaCl dilution buffer and one wash with dilution buffer without NaCl, the protein was eluted from
156 beads with elution buffer (dilution buffer, 250 mM NaCl, 0.2% SDS, 1% β-mercaptoethanol) over a 10-
157 minute incubation at 37°C, then denatured at 95°C for 5 minutes in 1X SLB with 1% β-mercaptoethanol
158 and stored at -20°C.

159 **2.4 SDS-PAGE and Western Blotting**

160 12% Bis-Tris polyacrylamide gels were run in 1X XT MOPS buffer (Bio-Rad #1610788) and transferred
161 onto nitrocellulose (to detect SQSTM1) or a polyvinylidene fluoride (to detect LC3-II) membranes via
162 semi-dry transfer using transfer buffer (192 mM glycine, 25 mM tris base, 20% methanol, 0.05% SDS)
163 and the Transblot Turbo Transfer System. Primary antibodies rabbit anti-SQSTM1 (1:1000; Cell Signaling
164 #D1Q5S) or rabbit anti-SQSTM1 (1:1000; Invitrogen #PA5-20839), rabbit anti-LC3A/B (1:1000; Cell
165 Signaling #D3U4C), and mouse anti-VCP (1:1000; Proteintech #60316-1-Ig) were used to detect SQSTM1,
166 LC3-II, and VCP, respectively. Secondary antibodies goat anti-rabbit Starbright 520 (1:2500; Bio-Rad
167 #12005870), donkey anti-rabbit Alexa Fluor 790 (1:2500; Jackson ImmunoResearch #711-655-152), and
168 goat anti-mouse Alexa Fluor 488 (1:2500; Jackson ImmunoResearch #115-545-003) were used. Tubulin-
169 rhodamine (1:5000; Bio-Rad #12004166) was used to detect tubulin as the loading control. Alexa Fluor
170 680 Streptavidin (1:5000; Jackson ImmunoResearch #016-620-084) was used to detect biotinylated
171 proteins.

172 **2.5 Fluorescence Microscopy**

173 For fixed cell imaging, cells were treated with 50 nM LysoTracker Deep Red (Invitrogen #L12492) for 1
174 hour prior to fixation. Cells were washed twice with 1X phosphate buffer saline (PBS), then fixed in 4%
175 paraformaldehyde for 20 minutes at room temperature. Again, cells were washed twice with 1X PBS,
176 then permeabilized in 1X PBS containing 0.1% TX-100, 1 µM $CaCl_2$, 1 µM $MgCl_2$ for 1 minute. Again, cells
177 were washed twice with 1X PBS, then blocked in 0.2% gelatin for 30 minutes. Next, cells were incubated
178 with the primary antibody for 1 hour. Rabbit anti-SQSTM1 (1:500; Invitrogen #PA5-20839) and mouse
179 anti-HTT (1:500; Millipore #MAB2166) were used to detect SQSTM1 and HTT, respectively. Cells were
180 washed twice with 0.2% gelatin, then the last step was repeated with the secondary antibody.
181 Secondary antibodies goat anti-rabbit Alexa Fluor 488 (1:500; Invitrogen) and donkey anti-mouse Alexa
182 Fluor 555 (1:500; Invitrogen) were used. Again, cells were washed twice with 0.2% gelatin, then

183 incubated in 1 µg/mL DAPI (Sigma #D9542) for 20 minutes. Finally, cells were washed twice with 0.2%
184 gelatin. The coverslips were mounted onto microscope slides (Fisher) using ProLong Gold Antifade
185 Mountant (Invitrogen #P36934) and sealed with nail polish. Using a Nikon AXR laser scanning confocal
186 microscope and its NIS-Elements software, Z-stack images were captured at 60X magnification. Next, 3D
187 Deconvolution was applied. Protein colocalization was determined by measuring Pearson Correlation
188 Coefficient (PCC) between channels. For HeLa cells, PCC was determined from regions of interest
189 manually drawn around single cells. For neurons, PCC was determined from regions of interest using the
190 automated General Analysis 3 (GA3).

191 **2.6 Molecular Docking**

192 Molecular docking prediction was performed using the AutoDock Vina program[31]. Briefly, the protein
193 PDBQT file was opened in AutoDockTools software to define the grid box dimensions. Molecular docking
194 was then performed using AutoDock Vina via the command prompt, specifying the file path to the
195 program and a folder containing the protein PDBQT file, the ligand PDBQT file, and a text file listing the
196 PDBQT file names, grid box dimension values, energy range, and exhaustiveness. Energy range was set
197 to 4 and exhaustiveness to 64. Running this program produced an "output.pdbqt" file containing the top
198 ligand binding conformations, along with a "log.txt" file listing the corresponding binding affinities.

199 **2.7 qPCR**

200 Total RNA from cells was extracted using RNAZol RT (Bioshop #RNN190). Then, 500 ng of total RNA was
201 used to prepare cDNA using High-Capacity cDNA Reverse Transcription Kit (Applied Biosystems
202 #4368813). Next, cDNA was diluted 1:5, and qPCR was performed using primers and the PowerTrack
203 SYBR Green Master Mix (Applied Biosystems #A46109). Each sample was run in triplicate. qPCR cycling
204 conditions were 2 minutes at 95°C, followed by 40 cycles of 5 seconds at 95°C and 30 seconds at 60°C,
205 then finally 15 seconds at 95°C, 1 minute at 60°C, and 15 seconds at 95°C. The forward and reverse
206 primer sequences were synthesized by IDT and are listed in Table 1. *ACTB* and *GAPDH* were used as

207 housekeeping genes. Primers for the ZDHHCs were previously published[32]. Primers for *SQSTM1*, *HTT*,

208 *VCP*, *MAP1LC3B*, the histone deacetylases, the serine hydrolases, and the housekeeping genes were

209 designed for this study.

210 **Table 1 List of Human Primers for qPCR**

Gene	Forward Sequence (5' to 3')	Reverse Sequence (5' to 3')
ACTB	GCCGCCAGCTCACCA	CTCGTCGCCCACATAGGAAT
GAPDH	TCGGAGTCAACGGATTTGGT	TTCCCGTTCTCAGCCTTGAC
ZDHHC1	CTCACCCGCTCCAGATTGTG	TGAGGCAGGAGGGGAACAAG
ZDHHC2	TGGAGAGAGAGCCAAGAGGAG	TTATAAGTTGGCATCTGTCACAGTATC
ZDHHC3	CTTAACTTCAGTTCGACAGAGTGC	GAAGAGCAGGCCCTCAAAGC
ZDHHC4	GATTGTCTTCATGCTGGGCTTTG	CTCTGTACCACTCGTTAGTAGTCTG
ZDHHC5	GAAGACTGAAGAAAGATAAGAGACATTG	GACACTTCAAAAGTTTACTGTGGATG
ZDHHC6	TCTGCTTGTCCTGGGCTGAG	TGTCTTGGTCTGAAACCCAACC
ZDHHC7	AGTCCATGCTCTGATCCTTTGTG	GGAAGATCAACAGGATTACAGTTATCG
ZDHHC8	TCTGTGACAACTGTGTAGAGGAC	AGCAGGAACAGGAAGAAGTAGC
ZDHHC9	TAGCAATTGGACTTTTGATGATGTTTG	GGGTTTTGCGATTACACGAGAG
ZDHHC11	TCCGTCACCCCAGAAGCCATAC	CGTGAGGCAGGAAGGGAATGAAG
ZDHHC12	TGCTGACCTGGGGAATCACG	CATGAGTGACACAGCGAGGTAG
ZDHHC13	GCATATCTCATCTCAAAGGGACAG	CAACCACATTGAGAGAAGGATTAAAC
ZDHHC14	TCGCTGGCATCCTGTTCTTC	TGCCGTTTGCGATATCTATTTGC
ZDHHC15	TATGAATGAGTCACAGAACCCACTGCTAG	TAATCTTGGTTGTCATCCTCGTTGTCTTCC
ZDHHC16	ATTGTAGCTATCGCCTACCTGTG	AGTAGTGGAAGACAATCAGGATCAG
ZDHHC17	ATGGTTGTGCAACTAATGAAATATGG	GCTATGAGATAAGCAACAATTGAGG
ZDHHC18	CCACCACCGGCCTCTTCTTC	GAGGATGGCAGCGATGATGG
ZDHHC19	GTCCCTGGTTCCTCCCTAGC	AATGCGAAGAAGAGGCCACTG
ZDHHC20	ATCAACCTTTTCCTATCAAACCACTTAG	GCCTTCTTCAGCTCCATTCTCC
ZDHHC21	TCTGGGAATTATGTAACAAGTGTAATTTG	AGAGCCAATGATTATCTTCACCAAC
ZDHHC23	AAAAGTGAACATCAGCATCATCCC	CCAGGAGGAAATGCCAGGAAG
ZDHHC24	CCCCTTCCGAGCTTCTATTGG	CTAGGCCGCTTCCGTATTGG
SQSTM1	GCACTACCGCGATGAGGAC	GCCATCGCAGATCACATTGG
HTT	GCATGGGATCCTGTCCCTTC	GGAGTGTATGGACACCTGGC
VCP	TCTGGAGCCGATTCAAAAGGT	TTCATCCATCTTGGGCTGGG
LYPLA1	CGCTCTTCCTTCCGCTTGC	GCAGGAAAATCACCGCAGC
LYPLA2	AGGCAGCAGAGAACATCAAGG	CAGGTGAGGGCCGTGTAGAG
LYPLAL1	CCTGCATGGCTCAGGTGATT	TCAAGGTGTTCTGGGCAGTC
PPT1	GAAGACCCTGATGGAGGACG	GATCATGGGAGGTGAAGGGC
PPT2	AGACCATCCCAATGCCACAG	CCCGCAGATAAACCAGTTGC
ABHD10	AGCTGATGGGCCACAGATTC	GCATGCTCCACACACCTTTC
ABHD16A	CTCCTGCAGCATCGGTATCC	CGTGTTCTGCCTGGTAGGAG
ABHD17B	TTGCTCTTAGGACAAGATATGGC	ATCAGGAAAGGCAACTCGC

ABHD17C	TTCTACATTGGCCTCGGCTC	GACTCACGCCATACCGGG
HDAC1	TCTATCGCCCTCACAAAGCC	CTCACCAACGTTGAATCTCTGC
HDAC2	GTGAGATTCCCAATGAGTTGCC	GGTGCATGAGGTAACATGCG
HDAC3	ACTACTGTCTGAACGTGCCC	ATTCAACGCATTCCCCATGC
HDAC6	CTATGTCCACCACCAGGCTC	CCCTCATCCAAGGTACAGGC
MAP1LC3B	GCTCATCAAGATAATTAGAAGGCG	GTCTCCTGGGAGGCATAGAC

211 **2.8 Mice**

212 YAC128 transgenic mice on an FVB/N genetic background were obtained from in-house breeding
213 colonies and were originally purchased from the Jackson Laboratory (Strain ID: 004938). Mice were
214 housed in standard laboratory cages under a 12-hour light/dark cycle at 23 ± 1°C, with *ad libitum* access
215 to food and water, and toys for enrichment. All mouse experiments were conducted in accordance with
216 Animal Use Protocol #44651, approved by the UW Animal Care Committee. Mice were administered
217 Vorinostat once every second day between 10 am and 12 pm, at a dose of 50 mg/kg through
218 intraperitoneal (IP) injection (alternating right and left side) for four consecutive weeks for a total of 15
219 treatments[33]. Vorinostat was dissolved in DMSO at a concentration of 40 mg/mL and stored at -20°C. On
220 the day of IP injection, the stock was diluted in corn oil to yield a working solution containing 18.75%
221 DMSO and 81.25% corn oil, with a final Vorinostat concentration of 7.5 µg/µL. Control injections
222 contained the same DMSO-to-corn oil ratio. Solutions were warmed to 37°C for 5 minutes and vortexed
223 for 15 seconds prior to IP injection.

224 **2.9 Mouse-Derived Primary Cortical Neurons**

225 Primary cortical neurons were derived from YAC128 mouse embryos at embryonic day 17. Cortices were
226 dissociated using papain and seeded on 1 mg/mL poly-L-lysine coated wells or glass coverslips (#1.5;
227 Warner) in 6-well plates at 280,000 and 180,000 neurons per well for biochemistry and microscopy
228 experiments, respectively. Neurons were plated in plating media [neurobasal media (Gibco #21103049)
229 supplemented with 2.5% FBS, 2.5% horse serum, 2 mM L-glutamine, 1X penicillin-streptomycin, 2%
230 B27]. The next day, plating media was replaced with neuronal media (neurobasal media supplemented

231 with 2 mM L-glutamine, 1X penicillin-streptomycin, 2% B27). Neurons were processed at 17 days *in*
232 *vitro*.

233 **2.10 Statistics**

234 Statistical analyses and biological repeats are indicated in figure legends. Significant outliers identified
235 using the Grubbs' test were removed and are indicated in figure legends. GraphPad Prism 10 was used
236 for all statistical analyses and graph preparation. Graphs are presented as the standard error of the
237 mean.

238 ## 3. Results

239 **3.1 Vorinostat increases SQSTM1 palmitoylation but does not affect total protein**
240 **palmitoylation**

241 An acyl-biotin exchange (ABE) assay was performed on HeLa cells overexpressing SQSTM1-HA and
242 treated with 10 µM Vorinostat or 10 µM PalmB. PalmB is a non-specific inhibitor of depalmitoylating
243 enzymes[34], whereas 2BP is a non-specific inhibitor for palmitoylation[35]. The absence of signal in the
244 hydroxylamine (HAM-) lane confirms that without thioester bond cleavage, biotin-HPDP cannot be
245 incorporated on free cysteine residues. Vorinostat treatment led to a significant increase in SQSTM1
246 palmitoylation (*$p<0.05$) (Figure 2A,B), while PalmB treatment led to no changes.

247

248 Next, we performed a click chemistry assay on HeLa cells treated with 10 µM Vorinostat, 10 µM ML348,
249 10 µM PalmB, or 50 µM 2BP. ML348 is a specific inhibitor for APT1[34], the enzyme that depalmitoylates
250 SQSTM1[15,24]. Vorinostat treatment led to no changes in total protein palmitoylation (Figure 2C,D).
251 ML348 and 2BP treatments led to a slight decrease in total protein palmitoylation, whereas PalmB led to
252 a slight increase. The absence of a signal in the cold palmitate (palm) lane confirms that without an
253 alkyne group, biotin-azide cannot be incorporated on the palmitate.

254

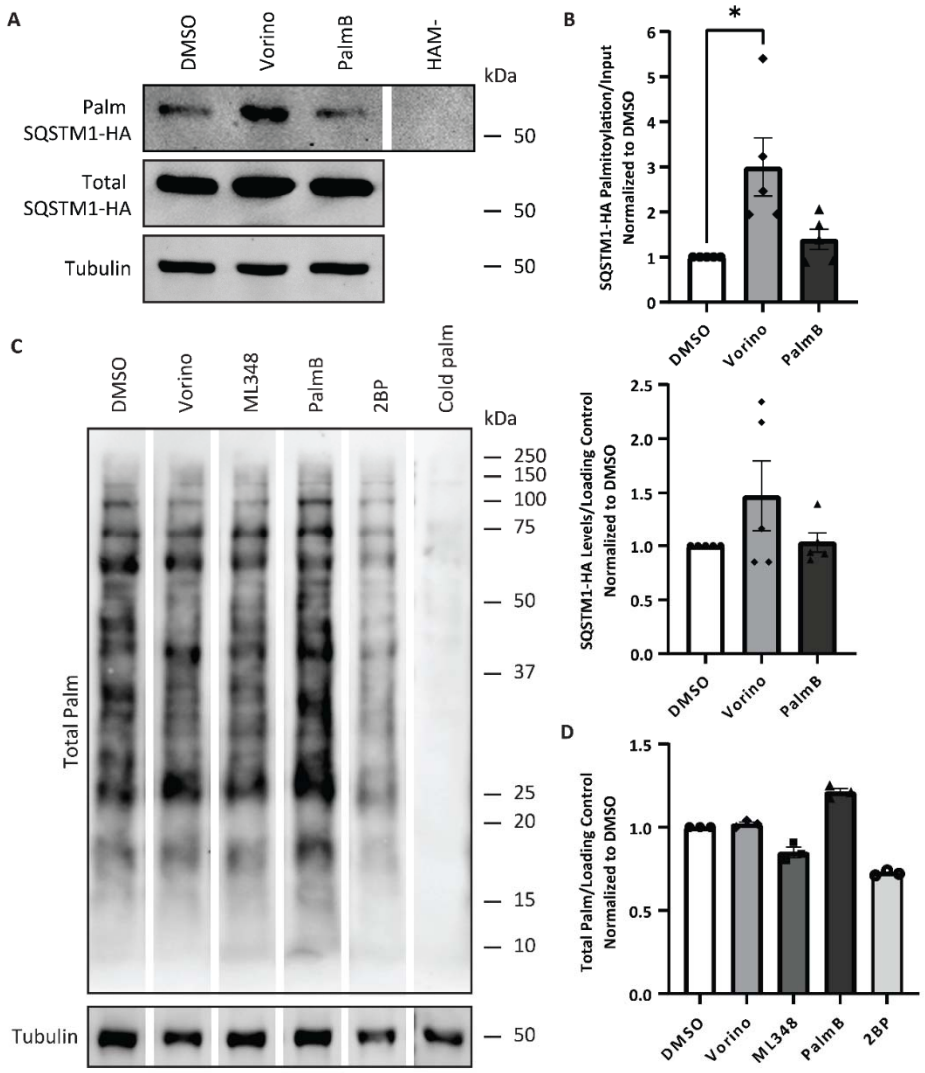

Figure 2 – Vorinostat increases SQSTM1 palmitoylation but does not affect total protein palmitoylation. (A) SQSTM1 palmitoylation was detected via acyl biotin exchange and is sensitive to Vorinostat treatment in HeLa cells. Composite of the same gel. **(B)** Quantification of (top) SQSTM1 palmitoylation and (bottom) SQSTM1 levels from five biological replicates. Kruskal-Wallis test followed by Dunn's post-hoc analysis. **(C)** Total palmitoylated protein was detected via click chemistry and is not sensitive to Vorinostat treatment. Composite of the same gel. **(D)** Quantification of total palmitoylated protein from three biological replicates. Kruskal-Wallis test followed by Dunn's post-hoc analysis.

22-month-old YAC128 mice were administered 50 mg/kg Vorinostat via intraperitoneal injection once every second day for four consecutive weeks. Subsequently, an ABE was performed on approximately 30 mg of ground cortices. Vorinostat treatment in YAC128 mice led to a significant increase in SQSTM1 and VCP palmitoylation (*$p<0.05$) compared to YAC128 DMSO-treated and WT Vorinostat-treated mice

268 (Figure 3A,B). Vorinostat treatment in WT mice led to no changes in SQSTM1 and VCP palmitoylation.

269 Vorinostat treatment led to no changes in total protein palmitoylation in both WT and YAC128 mice.

270

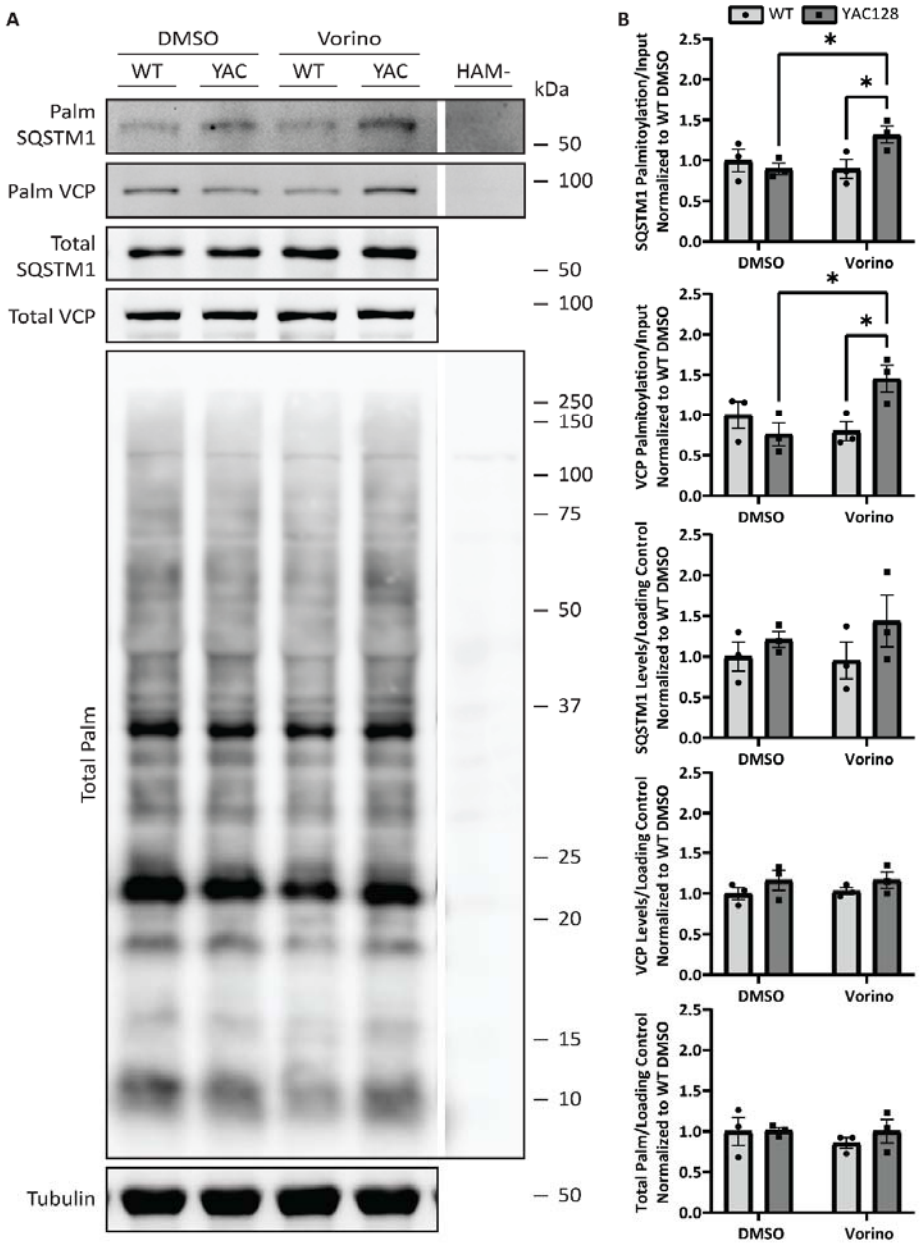

271

272 **Figure 3 – Vorinostat crosses the blood-brain barrier and increases SQSTM1 palmitoylation in YAC128**
273 **mice. (A)** SQSTM1 palmitoylation in cortices was detected via acyl biotin exchange and is sensitive to
274 Vorinostat treatment in YAC128 mice. Composite of the same gel. **(B)** Quantification of (top) SQSTM1
275 palmitoylation, (second) VCP palmitoylation, (third) SQSTM1 levels, (fourth) VCP levels, and (bottom)
276 total palmitoylated protein from three biological replicates. Two-way ANOVA test followed by Fisher's
277 LSD post-hoc analysis (*$p<0.05$).

278

279 **3.2 Vorinostat enhances autophagy and loading of mHTT aggregates into autophagosomes**

280 In autophagy, SQSTM1 is degraded in autophagolysosomes, and while some of LC3-II located on the
281 inner surface is also degraded, the majority located on the outer surface is recycled back to LC3-I, the
282 inactive delipidated form of LC3[36]. This makes SQSTM1 and LC3-II excellent markers of autophagy, such
283 that increased autophagic flux is indicated by reduced SQSTM1 levels and elevated LC3-II levels[36]. BafA1
284 is a late-stage autophagy inhibitor that prevents autophagosome-lysosome fusion leading to an increase
285 in both SQSTM1 and LC3-II levels[36]. BafA1 is used to confirm that the effect of the drug treatment on
286 autophagic flux is indeed a result of increased autophagy[36]. For example, if SQSTM1 levels decrease and
287 LC3-II levels increase with drug treatment, but do not substantially increase with drug plus BafA1
288 treatment, this suggests that the drug treatment blocks autophagic flux, rather than increases it[36].

289

290 HeLa cells were treated with 10 µM Vorinostat, 10 µM ML348, or 10 µM PalmB, with or without BafA1.
291 Vorinostat treatment led to a significant decrease in SQSTM1 levels (*$p<0.05$) (Figure 4A,B). In addition,
292 Vorinostat treatment significantly increased LC3-II levels (*$p<0.05$). ML348 and PalmB treatment led to
293 no changes in SQSTM1 or LC3-II levels. All BafA1 treatment conditions led to a significant increase in
294 LC3-II (**$p<0.01$) and SQSTM1 (***$p<0.001$).

295

296 Furthermore, a key characteristic of autophagy is the colocalization of SQSTM1, HTT, and lysosomes,
297 which suggests that SQSTM1 is successfully delivering cargo (*e.g.,* mHTT) with the support of HTT to
298 autophagosomes, which fuse with lysosomes to form autophagolysosomes. Therefore, increased
299 colocalization between these proteins and organelles, as measured by the PCC, indicates enhanced
300 autophagic flux, as the presence of SQSTM1 and HTT in lysosomes signifies their successful delivery.
301 HeLa cells were treated with 10 µM Vorinostat, 10 µM ML348, or 10 µM PalmB and visualized by fixed

302 cell confocal microscopy. When treated with Vorinostat, ML348, or PalmB, SQSTM1 and HTT
303 colocalization significantly increased, with a more pronounced increase elicited by Vorinostat
304 (****p<0.0001) (Figure 4C,D). When treated with Vorinostat or PalmB, SQSTM1 and lysosome
305 colocalization significantly increased, with a more pronounced increase elicited by Vorinostat
306 (****p<0.0001). Finally, when treated with Vorinostat or PalmB, HTT and lysosome colocalization
307 significantly increased, with a more pronounced increase elicited by Vorinostat (****p<0.0001). In
308 another experiment, primary cortical neurons derived from WT and YAC128 mice were treated with 10
309 μM Vorinostat, 10 μM ML348, or 10 μM PalmB and visualized by fixed cell confocal microscopy. In WT
310 cortical neurons treated with Vorinostat, SQSTM1 and HTT colocalization was not affected (Figure 5A,C).
311 However, in YAC128 cortical neurons treated with Vorinostat, SQSTM1 and mHTT colocalization
312 significantly increased (***p<0.001). Similarly, SQSTM1 and lysosome colocalization was not affected
313 with Vorinostat treatment in WT cortical neurons but significantly increased (**p<0.01) in YAC128
314 cortical neurons. In addition, HTT and lysosome colocalization, which includes both HTT and mHTT, was
315 not affected with Vorinostat treatment in WT cortical neurons but significantly increased
316 (****p<0.0001) in YAC128 cortical neurons, which is especially relevant in this context where
317 colocalization suggests that mHTT aggregates are in autophagolysosomes. When treated with ML348,
318 WT cortical neurons showed significantly increased SQSTM1 and mHTT colocalization (**p<0.01),
319 whereas YAC128 cortical neurons showed significantly increased SQSTM1 and mHTT colocalization, as
320 well as HTT and lysosome colocalization (***p<0.001 and **p<0.01, respectively). When treated with
321 PalmB, WT cortical neurons showed significantly increased SQSTM1 and mHTT, as well as HTT and
322 lysosome colocalization (**p<0.01 and ****p<0.0001, respectively), whereas YAC128 cortical neurons
323 showed significantly increased HTT and lysosome colocalization (***p<0.001).
324

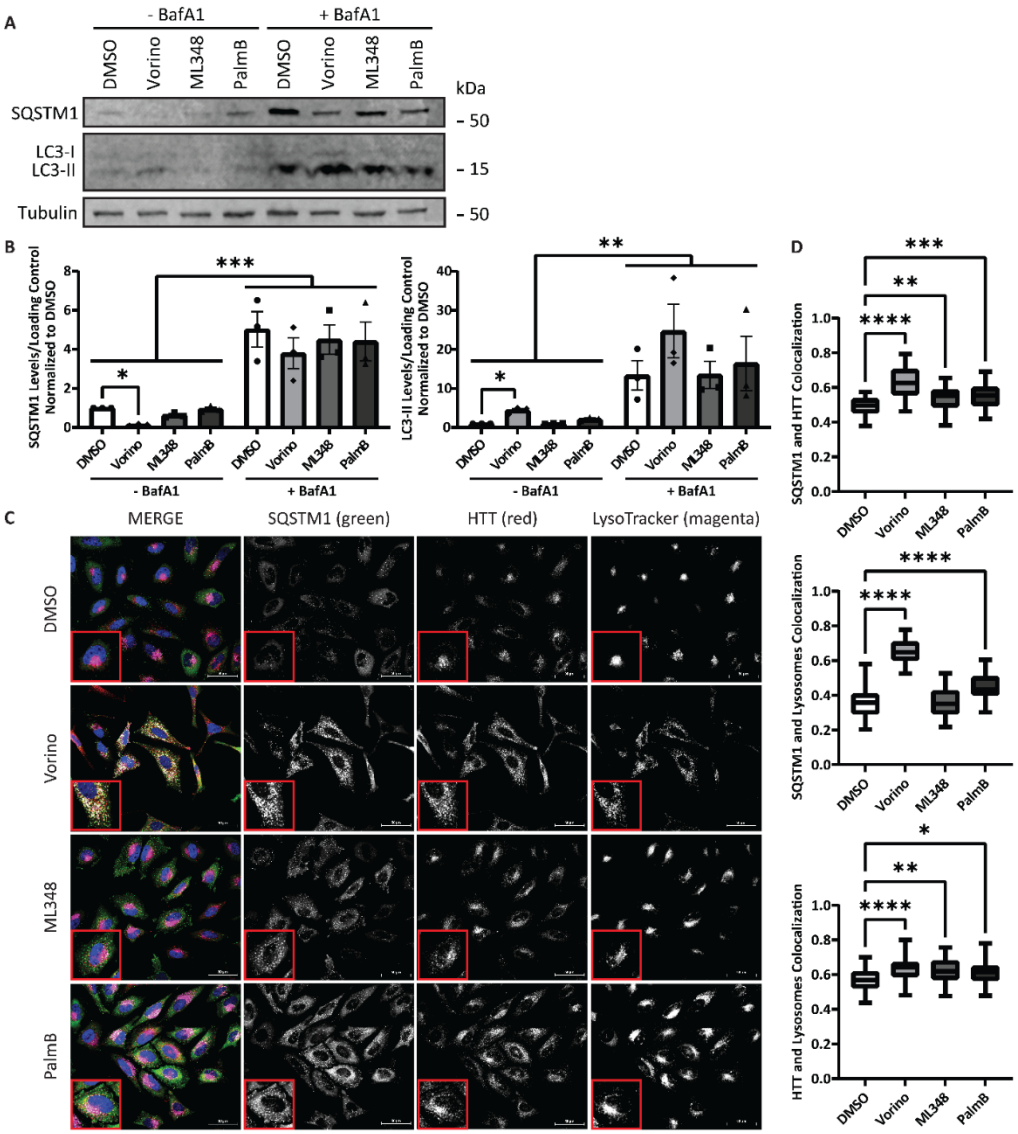

Figure 4 – Vorinostat increases autophagic flux. (A) SQSTM1 and LC3-II levels were detected and are sensitive to Vorinostat treatment in HeLa cells. **(B)** Quantification of (left) SQSTM1 levels and (right) LC3-II levels from three biological replicates. Kruskal-Wallis test followed by Dunn's post-hoc analysis (*p<0.05) within +/- BafA1 conditions. Two-way ANOVA test followed by Fisher's LSD post-hoc analysis (**p<0.01, ***p<0.001) across BafA1 conditions. **(C)** Vorinostat affects SQSTM1, HTT, and lysosome colocalization levels in HeLa cells. **(D)** Quantification of (left) PCC between SQSTM1 and HTT, (middle) PCC between SQSTM1 and lysosome, and (right) PCC between HTT and lysosome, 15 cells per condition from three biological replicates. One-way ANOVA test followed by Dunnett's post-hoc analysis (*p<0.05, **p<0.01, ***p<0.001, ****p<0.0001). Box and whiskers (min to max).

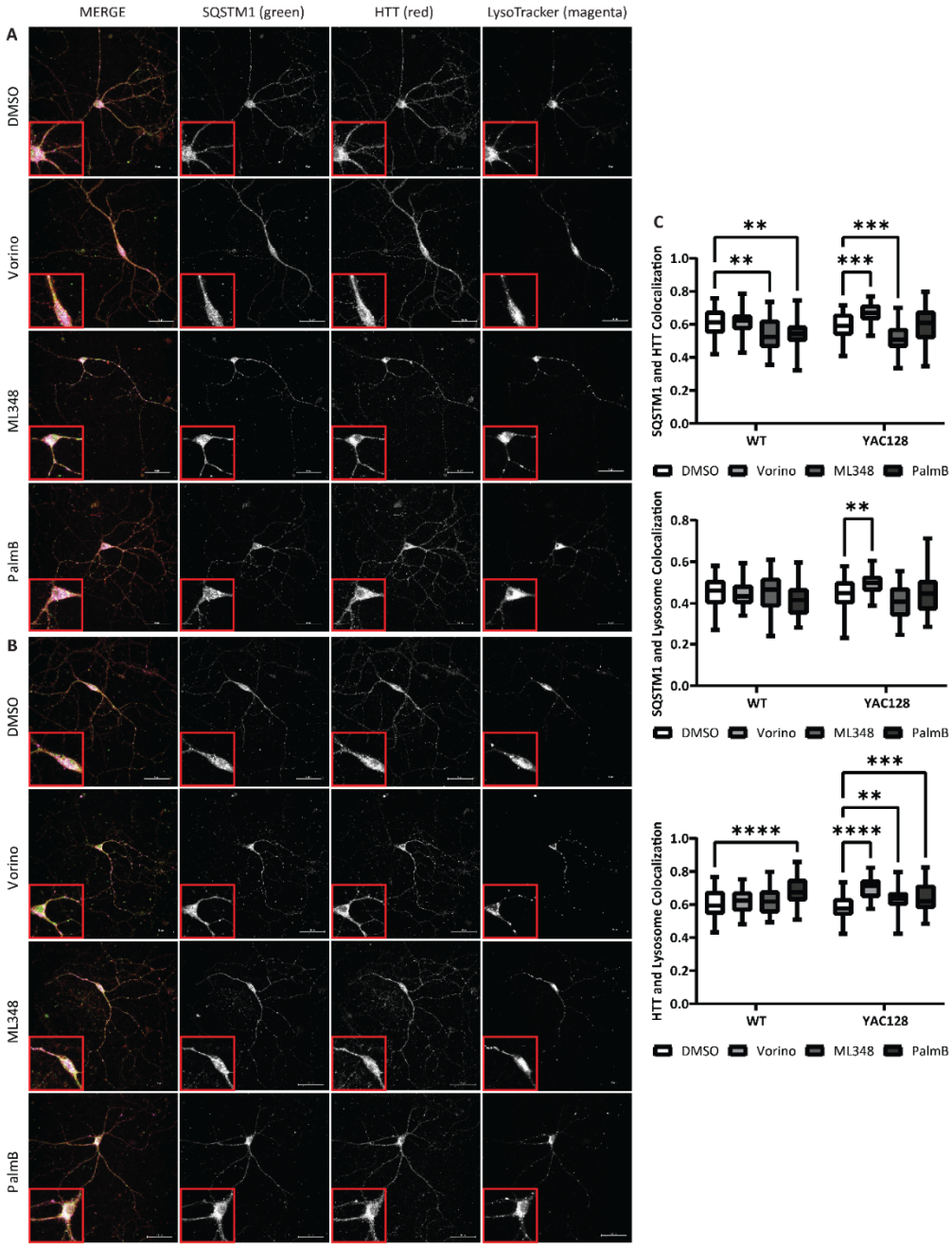

Figure 5 – Vorinostat redirects mHTT and SQSTM1 to lysosomes in HD neurons. (A) SQSTM1, HTT, and lysosome colocalization in primary cortical neurons derived from WT mice. **(B)** Vorinostat significantly increases SQSTM1 and mHTT co-localization, and lysosome colocalization with SQSTM1 and mHTT in primary cortical neurons derived from YAC128 HD mouse embryos. **(C)** Quantification of (top) PCC between SQSTM1 and HTT, (middle) PCC between SQSTM1 and lysosome, and (bottom) PCC between HTT and lysosome, on an average of 15 neurons per condition from three biological replicates. Two-way ANOVA test followed by Dunnett's post-hoc analysis (**p<0.01, ***p<0.001, ****p<0.0001). Box and whiskers (min to max).

346 **3.3 Vorinostat may function as a depalmitoylation inhibitor and transcriptional regulator**

347 SQSTM1 has been shown to be depalmitoylated by APT1[15,24]. Thus, our initial theory was Vorinostat may
348 function via inhibition of APT1, thereby increasing SQSTM1 palmitoylation. To further investigate,
349 molecular docking experiments were performed using AutoDock Vina. These results indicate that
350 ML348, an inhibitor specific to APT1[34], and Vorinostat have a deep fit into the binding pocket of APT1,
351 with ML348 exhibiting a stronger binding affinity (-10.6 kcal/mol) compared to Vorinostat (-8.0 kcal/mol)
352 (Figure 6A). We also looked at APT2 for comparison and found that ML349, an inhibitor specific to
353 APT2[34], and Vorinostat have a deep fit into the binding pocket of APT2, with ML349 exhibiting a stronger
354 binding affinity (-12.9 kcal/mol) compared to Vorinostat (-8.0 kcal/mol). For context, the more negative
355 the value, the stronger the binding affinity.

356

357 Alternatively, Vorinostat is already known as an HDAC inhibitor, so its function could be through
358 increasing the transcription of palmitoylating enzymes or decreasing the transcription of
359 depalmitoylating enzymes. To further investigate, qPCR was performed on HeLa cells treated with 10
360 μM Vorinostat to quantify the relative transcript levels of *ZDHHC1-24*, *SQSTM1*, *HTT*, *VCP*, *LYPLA1*
361 (APT1), *LYPLA2* (APT2), *PPTs*, *ABHD*s, *HDAC*s, and *MAP1LC3*s (Figure 6B,C). Compared to DMSO,
362 treatment with Vorinostat led to significantly increased *ZDHHC11*, *ZDHHC23*, and *SQSTM1* transcript
363 levels, as well as significantly decreased transcript levels of *ZDHHC2*, *ZDHHC4*, *ZDHHC5*, *ZDHHC9*,
364 *ZDHHC16*, *ZDHHC17*, *ZDHHC18*, *ZDHHC20*, *ZDHHC21*, *VCP*, *LYPLA2*, *PPT1, PPT2*, *ABHD16A,* and *ABHD17C*.
365 Notably, *HTT*, *LYPLA1*, and *ZDHHC19* transcript levels were unaffected by Vorinostat treatment.
366 ZDHHC22 had amplification in the Vorinostat condition, but not DMSO condition, whereas ABHD17A and
367 MAP1LC3A showed no amplification in either condition.

368

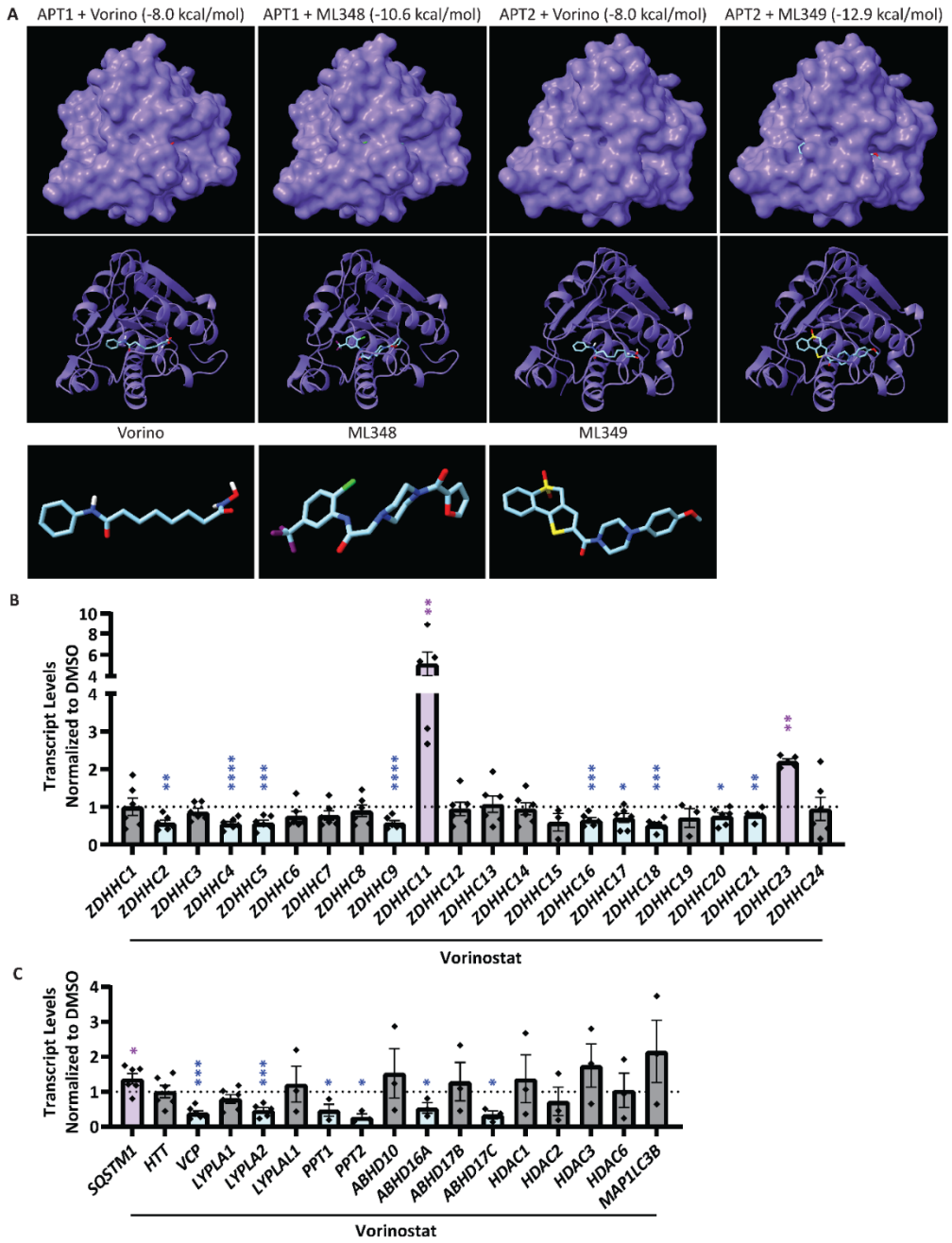

Figure 6 – Vorinostat may function as a depalmitoylation inhibitor and transcriptional regulator. (A) Vorinostat and ML348 molecular docking and binding affinity on APT1 and APT2 were predicted using AutoDock Vina. **(B)** *ZDHHC1-24* transcript levels were detected via qPCR in HeLa cells. *ZDHHC2,4,5,9,11,16,17,18,20,21,23* transcript levels are sensitive to Vorinostat treatment. One significant outlier (SO) removed from ZDHHC11 and ZDHHC23. Two-tailed unpaired *t*-test (*p<0.05, **p<0.01, ***p<0.001, ****p<0.0001). **(C)** *SQSTM1*; *HTT; VCP*; *LYPLA1,2*; *LYPLAL1*; *PPT1,2*; *ABHD10,16A,17A,17B,17C*; *HDAC1,2,3,6*; and *MAP1LC3A,B* transcript levels were detected via qPCR in HeLa cells. *SQSTM1*, *VCP*, *LYPLA2*, *PPT1*, *PPT2*, *ABHD16A*, and *ABHD17C* transcript levels are sensitive to Vorinostat treatment. One SO removed from LYPLA2. Two-tailed unpaired *t*-test (*p<0.05, ***p<0.001).

379 ## 4. Discussion

380 A hallmark of HD is the cytotoxic accumulation and aggregation of mHTT, which is partly caused and
381 subsequently exacerbated by dysfunctional autophagy. Our focus is failure at the cargo-loading step,
382 wherein SQSTM1 is unable to deliver cargo, mainly, mHTT aggregates, to the phagophore membrane for
383 degradation. Since palmitoylation plays an important role in protein localization to membranes, we
384 predict that the autophagic dysfunction seen in HD may be a result of reduced SQSTM1 palmitoylation,
385 which our group has confirmed previously in the brains of HD patients and YAC128 mice. Consequently,
386 we aim to promote mHTT intracellular degradation, thereby preventing cytotoxicity and neuronal death,
387 by restoring SQSTM1 palmitoylation. Through a high-throughput screening of FDA-approved drugs, we
388 identified blood-brain permeable Vorinostat as a candidate to increase SQSTM1 palmitoylation.

389

390 We found that Vorinostat treatment significantly increases SQSTM1 palmitoylation does not affect total
391 protein palmitoylation both *in vitro* (Figure 2) and *in vivo* (Figure 3). Since the biochemical assays for our
392 *in vivo* work were conducted on cortical tissue, this confirms that Vorinostat successfully crosses the
393 blood-brain barrier. Notably, PalmB did not increase SQSTM1 palmitoylation *in vitro*. This may be
394 because PalmB is a non-selective inhibitor of depalmitoylating enzymes. Since many palmitoylating
395 enzymes undergo regulatory palmitoylation (*e.g.,* ZDHHC6 is palmitoylated by ZDHHC16[37] and ZDHHC5 is
396 palmitoylated by ZDHHC20[38]), broad inhibition of depalmitoylating enzymes could disrupt the function
397 of palmitoylating enzymes, potentially explaining the lack of effect of PalmB on SQSTM1 palmitoylation.

398

399 With an increase in SQSTM1 palmitoylation induced by Vorinostat treatment, we then observed a
400 corresponding increase of autophagic flux. We found that Vorinostat treatment significantly decreases
401 SQSTM1 levels and increases LC3-II levels (Figure 4). SQSTM1 and LC3-II are autophagy markers, and
402 their respective decrease and increase in levels suggests increased autophagic flux, since SQSTM1 is
403 degraded in autophagolysosomes, whereas the majority of LC3-II is recycled back into the inactive

404 delipidated form of LC3. Increased autophagic flux was confirmed with Vorinostat plus BafA1 treatment,
405 a late-stage autophagy inhibitor[36], which significantly increased SQSTM1 and LC3-II levels.
406
407 Furthermore, with an increase in SQSTM1 palmitoylation induced by Vorinostat treatment, we then
408 observed a corresponding enhancement of autophagy. We found that Vorinostat treatment significantly
409 increased SQSTM1, mHTT, and lysosome colocalization in HeLa cells (Figure 4), as well as primary
410 cortical neurons derived from YAC128 mice, but not WT mice (Figure 5). In HeLa cells, this suggests
411 enhanced SQSTM1 and HTT delivery to autophagosomes. In YAC128 primary cortical neurons, increased
412 SQSTM1, mHTT, and lysosome colocalization suggests improved delivery of cytotoxic mHTT aggregates
413 to autophagosomes for subsequent degradation in autophagolysosomes, repairing the hallmark
414 neuropathological feature of HD. Notably, the observation that Vorinostat had an effect in YAC128 but
415 not in WT primary cortical neurons is important as it suggests that Vorinostat may exert its effects
416 selectively under pathological conditions, reducing the risk of potential off-target effects. The effects of
417 ML348 and PalmB on SQSTM1, mHTT, and lysosome colocalization were neither as strong, consistent,
418 nor specific as those of Vorinostat, suggesting that Vorinostat may be a more effective drug in HD.
419
420 Initially, we predicted that Vorinostat increases SQSTM1 palmitoylation by acting as a depalmitoylation
421 inhibitor, specifically of APT1, the depalmitoylating enzyme of SQSTM1. Consequently, we aimed to
422 better understand Vorinostat's ability to inhibit depalmitoylating enzymes through molecular docking
423 experiments to quantify Vorinostat's binding affinity to APT1 and APT2 (Figure 6). Although Vorinostat
424 had a deep fit into the binding pockets of both APT1 and APT2, its binding affinity to either was weaker
425 than that of the specific inhibitors, ML348 and ML349. However, prior experiments indicated that
426 Vorinostat was more effective than ML348 at increasing SQSTM1 palmitoylation, thus prompting us to
427 reassess our previous thinking. Vorinostat is also a known HDAC inhibitor, promoting histone acetylation
428 or transcription factor acetylation, thereby increasing transcription. Either way, Vorinostat could

429 increase the transcription of *ZDHHC* genes, leading to increased SQSTM1 palmitoylation through an
430 alternative pathway. Therefore, Vorinostat may be acting via a dual mechanism, as summarized in
431 Figure 7.
432

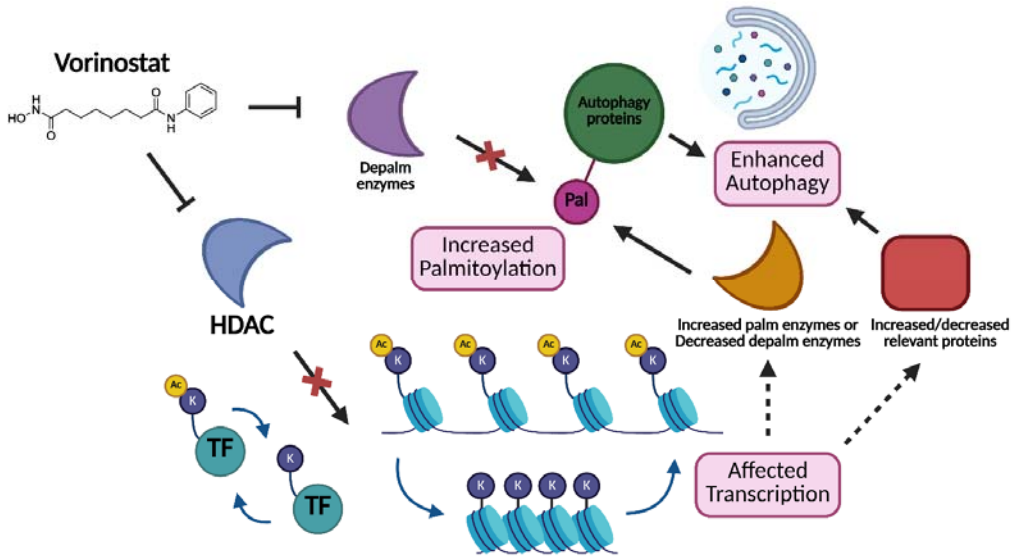

433
434 **Figure 7 – Predicted Vorinostat mechanism.** Vorinostat may be working through two concurrent
435 mechanisms to increase autophagy protein palmitoylation: inhibition of depalmitoylating (depalm)
436 enzymes and inhibition of acetylation enzymes (HDAC). Inhibition of depalmitoylating enzymes prevents
437 the depalmitoylation of SQSTM1, thus increasing SQSTM1 palmitoylation. In contrast, inhibition of HDAC
438 prevents deacetylation of histones, thus increasing their acetylation, promoting active transcription by
439 opening chromatin. Alternatively, inhibition of HDAC prevents deacetylation of transcription factors (TF),
440 thus increasing their acetylation, also promoting active transcription. K represents a lysine residue
441 protruding from the histone, and Ac represents an acetyl group. This may increase transcription of
442 palmitoylating (palm) enzymes or decrease the transcription of depalmitoylating enzymes, overall
443 increasing autophagy protein palmitoylation. Alternatively, this may increase or decrease transcription
444 of relevant proteins, such as SQSTM1, which may also enhance autophagy. Figure generated on
445 BioRender.
446

447 The next step was to confirm whether Vorinostat increases transcription of relevant proteins by
448 quantifying transcript levels via qPCR. We found that Vorinostat significantly increases *SQSTM1*
449 transcript levels compared to DMSO, suggesting that Vorinostat may promote autophagy. However,
450 Vorinostat plus BafA1 did not lead to an increase in SQSTM1 levels (Figure 4). It could be that Vorinostat

451 plus BafA1 leads to the accumulation of detergent-insoluble SQSTM1, as described by the Yang group[24],
452 which may limit detection of SQSTM1 via western blot. In addition, we found that Vorinostat
453 significantly increases *ZDHHC11* and *ZDHHC23* transcript levels compared to DMSO. Work by the Liu
454 group suggests that ATG2A is palmitoylated by ZDHHC11 and its *depalmitoylation* is required for proper
455 autophagosome formation[39]. In contrast, studies by the Kim group suggest that MCOLN3/TRPML3 is
456 palmitoylated by ZDHHC11 and its *palmitoylation* is required for proper autophagosome formation[40].
457 Minimal connections between ZDHHC23 and autophagy have been established. Therefore, it remains
458 unclear how Vorinostat-induced increases in the *ZDHHC11* and *ZDHHC23* transcript levels might have a
459 role in the increase and enhanced autophagy we observed following Vorinostat treatment. Furthermore,
460 we found that Vorinostat decreases *LYPLA2* transcript levels which encode APT2. APT2 depalmitoylates
461 HTT, and HTT palmitoylation is reduced in HD mouse models[18]. Therefore, reducing APT2 may increase
462 HTT palmitoylation, thereby lowering mHTT aggregation and cytotoxicity. Although increased transcript
463 levels do not necessarily equate to increased protein levels, they serve as a good representation of
464 potential regulatory changes at the transcriptional level and can provide insight into upstream effects of
465 Vorinostat treatment.
466
467 **4.1 Vorinostat and Huntington disease**
468 Vorinostat has been tested in HD mouse models previously, but in the context of its HDAC inhibiting
469 properties and fixing transcriptional dysregulation found in HD. The Bates group treated R6/2 HD mouse
470 model and found improved motor impairment, reduced mHTT aggregates in the cortex, and restored
471 *Bdnf* transcript levels[33,41]. BDNF is implicated in HD pathogenesis[42]. In R6/2 mice, *Bdnf* transcript levels
472 decline during disease progression[43]; accordingly, BDNF over-expression was found to improve HD
473 phenotypes[44]. The Bates group also found that Vorinostat decreases HDAC2 and HDAC4 levels *in vivo*[41].
474 In R6/2 mice, the group reported that HDAC4 associates with mHTT in a polyQ-dependent manner and
475 co-localizes with cytoplasmic inclusions, and knockdown of HDAC4 reduced cytoplasmic aggregate

476 formation, restored *Bdnf* transcript levels, rescued membrane properties of MSNs and of corticostriatal
477 synaptic transmission, improved motor and neurological impairment, and extended the lifespan of R6/2
478 mice[45]. To further understand the mechanism of HDAC4, the Cristea group studied the interaction of
479 HDAC4 in the context of HD through multiomics and propose a potential model of the role for HDAC4 in
480 HD[46]. One notable finding from their study is the interaction between HDAC4 and VCP, which they also
481 found has minimal interaction in the Q20 WT mice and maximal interaction in the Q140 HD mice, an
482 interaction which increases with age. Combining this with our findings on VCP, it is possible that the
483 increased interaction between HDAC and VCP, and likely VCP acetylation[47], interferes with VCP
484 palmitoylation, thereby disrupting its normal function. By deceasing HDAC4 levels with Vorinostat, VCP
485 function may be restored.
486
487 **4.2 VCP and Huntington disease**
488 Our group has recently shown that VCP palmitoylation is significantly reduced in the brains of HD mouse
489 models. It is still unclear the effect of decreasing VCP palmitoylation in the context of HD; however, we
490 looked at whether Vorinostat also rescues VCP palmitoylation in addition to SQSTM1 palmitoylation. We
491 found that *in vivo* Vorinostat treatment significantly increases VCP palmitoylation. VCP is also involved in
492 autophagy initiation, and since autophagy membrane-dependent process, this suggests that VCP
493 palmitoylation may modulate its function in this pathway. Links between VCP and HD have already been
494 established. The Qi group identified VCP as a mHTT-binding protein on mitochondria, where it drives
495 excessing mitophagy, or the autophagic degradation of mitochondria[48]. Because palmitoylation is a key
496 regulator of protein localization, restoring VCP palmitoylation could potentially correct its
497 mislocalization, reducing VCP accumulation on mitochondria in HD mouse models.
498
499 **4.3 Future Directions**

500 Although studies have demonstrated positive outcomes of Vorinostat treatment in HD mouse models,
501 the broader consequences of HDAC inhibition remain an important consideration. Determining the
502 specific mechanism by which Vorinostat mediates these positive effects should be a priority, as this
503 knowledge could guide the design of more targeted small molecules. However, it is also possible that
504 Vorinostat's multi-functional nature contributes to its broad impact on various HD phenotypes, whether
505 through restoring protein palmitoylation, correcting transcriptional dysregulation, or both. This raises an
506 important question: in a devastating disease like HD, at what point do the positive effects of Vorinostat
507 outweigh the risks of potential off-target effects? If nothing else, Vorinostat may provide insight into HD
508 pathology and guide the identification of novel therapeutic targets, including protein palmitoylation and
509 autophagy. In this study, we reported that Vorinostat crossed the blood-brain barrier and increased
510 SQSTM1 palmitoylation *in vivo*, as well as increased and enhanced autophagy *in vitro*, facilitating mHTT
511 loading into autophagolysosomes for degradation.
512

513 ## Author Contributions:

514 YA prepared the first draft. YA prepared Figures 1-7. YA completed the experiments in Figures 2-6. FA
515 contributed to the SQSTM1 palmitoylation experiment in Figure 2. MR contributed to the qPCR
516 experiments in Figure 6. AD contributed to the docking experiments in Figure 6. FR helped with animal
517 studies including preparation of primary neuronal cultures. YA and DDOM edited the final draft.

518 ## Funding:

519 DDOM is supported by a Natural Sciences and Engineering Research Council Discovery Grant (RGPIN-
520 2019-04617) and Huntington Society of Canada Navigator Research Award. YA is supported by a
521 Canadian Institutes of Health Research Canada Graduate Scholarship Master's Award, University of
522 Waterloo President's Graduate Scholarship, Brain Canada Rising Star in ALS Research Award, and John E.
523 Thompson Biology Graduate Scholarship. AD is supported by a Huntington Society of Canada
524 Undergraduate Summer Fellowship. FR is supported by a Mitacs Accelerate Grant in collaboration with
525 Circumvent Pharmaceuticals Inc., Canadian Institutes of Health Research Postdoctoral Research Award,
526 and an Uplifting Athletes Young Investigator Draft Award in collaboration with Cure VCP Disease Inc.

527 ## Conflicts of Interest:

528 The authors declare no conflicts of interest.

529 ## Acknowledgements:

530 We would like to acknowledge that the University of Waterloo resides on the traditional territory of five
531 Indigenous communities, including the Ho-de-no-sau-nee-ga (Haudenosaunee), Mississaugas of the
532 Credit First Nation, Anishinabewaki, Attiwonderonk (Neutral), and Mississauga peoples, which is
533 situated on the Haldimand Tract, a land granted to the Six Nations, encompassing six miles on either
534 side of the Grand River. This land is home to many past, present, and future Indigenous peoples.

535 ## References

536 1. Fujikake, N., Shin, M. & Shimizu, S. Association Between Autophagy and Neurodegenerative
537 Diseases. *Front Neurosci* **12**, 255 (2018).
538 2. Ramzan, F., Abrar, F., Mishra, G. G., Liao, L. M. Q. & Martin, D. D. O. Lost in traffic: consequences of
539 altered palmitoylation in neurodegeneration. *Front. Physiol.* **14**, 1166125 (2023).
540 3. Wlodarczyk, J. *et al.* Altered Protein Palmitoylation as Disease Mechanism in Neurodegenerative
541 Disorders. *J. Neurosci.* **44**, e1225242024 (2024).
542 4. Parzych, K. R. & Klionsky, D. J. An Overview of Autophagy: Morphology, Mechanism, and Regulation.
543 *Antioxid Redox Signal* **20**, 460–473 (2014).
544 5. Pircs, K. *et al.* Distinct subcellular autophagy impairments in induced neurons from patients with
545 Huntington's disease. *Brain* **145**, 3035–3057 (2022).
546 6. Martinez-Vicente, M. *et al.* Cargo recognition failure is responsible for inefficient autophagy in
547 Huntington's disease. *Nat Neurosci* **13**, 567–576 (2010).
548 7. Walter, C. *et al.* Activation of AMPK-induced autophagy ameliorates Huntington disease pathology
549 in vitro. *Neuropharmacology* **108**, 24–38 (2016).
550 8. Ghosh, R. & Tabrizi, S. J. Clinical Features of Huntington's Disease. in *Polyglutamine Disorders* (eds
551 Nóbrega, C. & Pereira de Almeida, L.) 1–28 (Springer International Publishing, Cham, 2018).
552 doi:10.1007/978-3-319-71779-1_1.
553 9. The Huntington's Disease Collaborative Research Group. A novel gene containing a trinucleotide
554 repeat that is expanded and unstable on Huntington's disease chromosomes. *Cell* **72**, 971–983
555 (1993).
556 10. Kay, C. *et al.* Huntington disease reduced penetrance alleles occur at high frequency in the general
557 population. *Neurology* **87**, 282–288 (2016).
558 11. Saudou, F. & Humbert, S. The Biology of Huntingtin. *Neuron* **89**, 910–926 (2016).

559 12. Ochaba, J. *et al.* Potential function for the Huntingtin protein as a scaffold for selective autophagy.
560 *Proc Natl Acad Sci U S A* **111**, 16889–16894 (2014).
561 13. Rui, Y.-N. *et al.* Huntingtin Functions as a Scaffold for Selective Macroautophagy. *Nat Cell Biol* **17**,
562 262–275 (2015).
563 14. Martin, D. D. O., Ladha, S., Ehrnhoefer, D. E. & Hayden, M. R. Autophagy in Huntington disease and
564 huntingtin in autophagy. *Trends in Neurosciences* **38**, 26–35 (2015).
565 15. Abrar, F. *et al.* Reduced Palmitoylation of SQSTM1/p62 in Huntington Disease Is Associated With
566 Impaired Autophagy. *FASEB J* **39**, e70549 (2025).
567 16. Alshehabi, Y., Abrar, F. & Martin, D. D. O. Sequestering sequestosome 1 via S-acylation in
568 autophagy, Huntington disease, and beyond. *Autophagy Rep* **4**, 2547975 (2025).
569 17. Yanai, A. *et al.* Palmitoylation of huntingtin by HIP14is essential for its trafficking and function. *Nat*
570 *Neurosci* **9**, 824–831 (2006).
571 18. Lemarié, F. L. *et al.* Rescue of aberrant huntingtin palmitoylation ameliorates mutant huntingtin-
572 induced toxicity. *Neurobiology of Disease* **158**, 105479 (2021).
573 19. Chamberlain, L. H. & Shipston, M. J. The physiology of protein S-acylation. *Physiol Rev* **95**, 341–376
574 (2015).
575 20. Anwar, M. U. & van der Goot, F. G. Refining S-acylation: Structure, regulation, dynamics, and
576 therapeutic implications. *Journal of Cell Biology* **222**, e202307103 (2023).
577 21. Lemarié, F. L., Sanders, S. S., Nguyen, Y., Martin, D. D. O. & Hayden, M. R. Full-length huntingtin is
578 palmitoylated at multiple sites and post-translationally myristoylated following caspase-cleavage.
579 *Front Physiol* **14**, 1086112 (2023).
580 22. Martin, D. D. O. & Sanders, S. S. Let's get fat: emergence of *S* -acylation as a therapeutic target in
581 Huntington disease. *Biochemical Society Transactions* BST20231290 (2024)
582 doi:10.1042/BST20231290.

583 23. Martin, D. D. O. & Sanders, S. S. Let's get fat: emergence of S-acylation as a therapeutic target in
584 Huntington disease. *Biochemical Society Transactions* **52**, 1385–1392 (2024).
585 24. Huang, X. *et al.* S-acylation of p62 promotes p62 droplet recruitment into autophagosomes in
586 mammalian autophagy. *Mol Cell* **83**, 3485-3501.e11 (2023).
587 25. Virlogeux, A. *et al.* Increasing brain palmitoylation rescues behavior and neuropathology in
588 Huntington disease mice. *Science Advances* **7**, (2021).
589 26. Martin, D. D. O. *et al.* Identification of Novel Inhibitors of DLK Palmitoylation and Signaling by High
590 Content Screening. *Sci Rep* **9**, 3632 (2019).
591 27. Athira, K. V., Sadanandan, P. & Chakravarty, S. Repurposing Vorinostat for the Treatment of
592 Disorders Affecting Brain. *Neuromol Med* **23**, 449–465 (2021).
593 28. Verrillo, L., Di Palma, R., de Bellis, A., Drongitis, D. & Miano, M. G. Suberoylanilide Hydroxamic Acid
594 (SAHA) Is a Driver Molecule of Neuroplasticity: Implication for Neurological Diseases. *Biomolecules*
595 **13**, 1301 (2023).
596 29. Liao, L. M. Q., Gray, R. A. V. & Martin, D. D. O. Optimized Incorporation of Alkynyl Fatty Acid Analogs
597 for the Detection of Fatty Acylated Proteins using Click Chemistry. *J Vis Exp*
598 https://doi.org/10.3791/62107 (2021) doi:10.3791/62107.
599 30. Hayashi, T., Thomas, G. M. & Huganir, R. L. Dual Palmitoylation of NR2 Subunits Regulates NMDA
600 Receptor Trafficking. *Neuron* **64**, 213–226 (2009).
601 31. Trott, O. & Olson, A. J. AutoDock Vina: improving the speed and accuracy of docking with a new
602 scoring function, efficient optimization and multithreading. *J Comput Chem* **31**, 455–461 (2010).
603 32. McClafferty, H. & Shipston, M. J. siRNA Knockdown of Mammalian zDHHCs and Validation of mRNA
604 Expression by RT-qPCR. in *Protein Lipidation* (ed. Linder, M. E.) vol. 2009 151–168 (Springer New
605 York, New York, NY, 2019).

606 33. Hockly, E. *et al.* Suberoylanilide hydroxamic acid, a histone deacetylase inhibitor, ameliorates motor
607 deficits in a mouse model of Huntington's disease. *Proc Natl Acad Sci U S A* **100**, 2041–2046 (2003).
608 34. Virlogeux, A. *et al.* Increasing brain palmitoylation rescues behavior and neuropathology in
609 Huntington disease mice. *Sci Adv* **7**, eabb0799 (2021).
610 35. Davda, D. *et al.* Profiling targets of the irreversible palmitoylation inhibitor 2-bromopalmitate. *ACS*
611 *Chem Biol* **8**, 1912–1917 (2013).
612 36. Klionsky, D. J. *et al.* Guidelines for the use and interpretation of assays for monitoring autophagy
613 (4th edition)1. *Autophagy* **17**, 1–382 (2021).
614 37. Abrami, L. *et al.* Identification and dynamics of the human ZDHHC16-ZDHHC6 palmitoylation
615 cascade. *eLife* **6**, e27826 (2017).
616 38. Plain, F. *et al.* Control of protein palmitoylation by regulating substrate recruitment to a zDHHC-
617 protein acyltransferase. *Commun Biol* **3**, 411 (2020).
618 39. Zheng, W. *et al.* S-palmitoylation modulates ATG2-dependent non-vesicular lipid transport during
619 starvation-induced autophagy. *EMBO J* **44**, 2596–2619 (2025).
620 40. Kim, S. W. *et al.* Palmitoylation controls trafficking of the intracellular Ca2+ channel
621 MCOLN3/TRPML3 to regulate autophagy. *Autophagy* **15**, 327–340 (2018).
622 41. Mielcarek, M. *et al.* SAHA decreases HDAC 2 and 4 levels in vivo and improves molecular
623 phenotypes in the R6/2 mouse model of Huntington's disease. *PLoS One* **6**, e27746 (2011).
624 42. Zuccato, C. & Cattaneo, E. Role of brain-derived neurotrophic factor in Huntington's disease. *Prog*
625 *Neurobiol* **81**, 294–330 (2007).
626 43. Benn, C. L., Fox, H. & Bates, G. P. Optimisation of region-specific reference gene selection and
627 relative gene expression analysis methods for pre-clinical trials of Huntington's disease. *Mol*
628 *Neurodegener* **3**, 17 (2008).

629 44. Gharami, K., Xie, Y., An, J. J., Tonegawa, S. & Xu, B. Brain-derived neurotrophic factor over-
630 expression in the forebrain ameliorates Huntington's disease phenotypes in mice. *J Neurochem* **105**,
631 369–379 (2008).
632 45. Mielcarek, M. *et al.* HDAC4 reduction: a novel therapeutic strategy to target cytoplasmic huntingtin
633 and ameliorate neurodegeneration. *PLoS Biol* **11**, e1001717 (2013).
634 46. Federspiel, J. D., Greco, T. M., Lum, K. K. & Cristea, I. M. Hdac4 Interactions in Huntington's Disease
635 Viewed Through the Prism of Multiomics. *Mol Cell Proteomics* **18**, S92–S113 (2019).
636 47. Mori-Konya, C. *et al.* p97/valosin-containing protein (VCP) is highly modulated by phosphorylation
637 and acetylation. *Genes Cells* **14**, 483–497 (2009).
638 48. Guo, X. *et al.* VCP recruitment to mitochondria causes mitophagy impairment and
639 neurodegeneration in models of Huntington's disease. *Nat Commun* **7**, 12646 (2016).
640